Field-induced structural transition and irreversible domain detwinning in the antiferromagnet $Fe_{1.1}Te$

X. Fabrèges,[1,2] F. Duc,[1,*] T. Roth,[3] W. Knafo,[1] R. Viennois,[4] and C. Detlefs[3]

[1]*Laboratoire National des Champs Magnétiques Intenses, UPR 3228, CNRS-UPS-INSA-UGA, 143 Avenue de Rangueil, F-31400 Toulouse, France*

[2]*Laboratoire Léon Brillouin, UMR12 CEA-CNRS Bât 563 CEA Saclay, 91191 Gif sur Yvette Cedex, France*

[3]*European Synchrotron Radiation Facility, Boîte Postale 220, F-38043 Grenoble Cedex, France*

[4]*Institut Charles Gerhardt Montpellier, UMR 5253, Université Montpellier 2 and CNRS, F-34095 Montpellier, France*

(Received 24 January 2017; revised manuscript received 4 May 2017; published 22 May 2017)

Single-crystal x-ray diffraction in pulsed magnetic fields of up to 31 T was used to investigate the iron telluride antiferromagnet $Fe_{1.1}Te$, which is a parent of the Fe-based chalcogenide superconductors. At temperatures below the Néel temperature $T_N \simeq 60$ K, high magnetic fields perpendicular to the c axis lead to an irreversible detwinning of the crystal at the field H_R, where magnetocrystalline domains are selected by a moment reorientation process. Just below T_N, the onset of a structural transition at the critical field $H_C > H_R$, which delimits the antiferromagnet phase, indicates a partial restoration of the high-temperature tetragonal symmetry. The lattice and magnetic answers to an in-plane magnetic field are discussed, emphasizing the strength of magnetoelastic coupling in $Fe_{1.1}Te$.

DOI: 10.1103/PhysRevB.95.174434

I. INTRODUCTION

The interplay between structural and electronic properties is a central issue in the study of high-temperature superconductivity. An illustration of this interplay is nematicity, i.e., a breaking of the lattice rotational symmetry, which has been observed in the paramagnetic state of cuprate [1] and iron-based [2] superconductors. In these systems, electronic effects—instead of a pure structural effect—are suspected to drive nemacity. For instance, an orbital mechanism of nematicity has been proposed for FeSe [3–5]. Due to layered lattices, nematicity generally leads to the formation of domains that are related through crystallographic twin laws. A lattice distortion responsible for a crystal twinning is also observed in magnetically ordered parent phases of high-temperature superconductors. In the cuprates $YBa_2Cu_3O_{7-\delta}$ [6] and $La_{2-x}Sr_xCuO_4$ [7,8], and in the iron-based $Ba(Fe_{1-x}Co_x)_2As_2$ [9–13], $EuFe_2As_2$ [14,15], and $Fe_{1+y}Te_{1-x}S_x$ [16–18], the application of pressure or magnetic field was shown to be an efficient way to detwin a crystal by selecting domains with a given orientation.

The importance of magnetoelastic coupling has been particularly emphasized for iron-based materials [19,20]. Among them, the parent compounds $Fe_{1+y}Te$ of the iron chalcogenide superconductors $Fe_{1+y}Te_{1-x}Se_x$ [21,22] present one of the simplest layered structure of iron-pnictides and chalcogenides with rather unusual magnetic orders. The latter are strongly dependent on the excess y of Fe atoms, with the establishment of either a commensurate bicollinear antiferromagnetic order [23,24] below $T_N \simeq 57-70$ K for low Fe doping ($y \lesssim 11\%$–12%), or incommensurate spiral magnetic structure for higher Fe doping [25–27]. For low Fe doping, the magnetic transition is first order and coincides with a structural transition that lowers the crystal symmetry from tetragonal to monoclinic. In the antiferromagnet $Fe_{1.1}Te$ at $T < T_N \simeq 60$ K, a high magnetic field $\mathbf{H} \perp \mathbf{c}$ induces an irreversible steplike increase in the magnetization at the reorientation field H_R ($\mu_0 H_R = 48$ T at $T = 4.2$ K) related to a spin-flop-like reorientation of the antiferromagnetic moments [28]. At temperatures $T \lesssim T_N$, a kink in the magnetization is the signature of the antiferromagnetic borderline H_C.

Here we report a single-crystal x-ray diffraction experiment in pulsed magnetic fields of up to 31 T to explore the effects of magnetoelastic coupling in $Fe_{1.1}Te$. We present a direct experimental evidence for an irreversible domain selection, i.e., an irreversible crystal detwinning, which coincides with a reorientation of the antiferromagnetic moments at the magnetic field H_R. We also observe the onset of a structural transition at the critical antiferromagnetic field H_C, compatible with a high-field restoration of the tetragonal symmetry.

II. EXPERIMENTAL DETAILS

The single crystal of $Fe_{1.1}Te$ studied here, grown by a modified Bridgman method [29], is a thin platelet of $\sim 4 \times 2 \times 0.35$ mm^3 with the **c** axis normal to the plate. The interstitial iron concentration was determined previously by chemical analysis using energy dispersive x-ray spectrometry and refinement of single crystal x-ray diffraction data as reported in Ref. [28]. The sample, glued with GE varnish on the sample holder, was aligned so that the **a** and **c** axes of the high-temperature tetragonal phase were in the diffraction plane. Diffraction experiments were performed on the undulator beamline ID06, at the European Synchrotron Radiation Facility (Grenoble, France), using a MAXIPIX two-dimensional pixel detector [30]. A split-pair pulsed magnet and cryostat assembly specially designed for x-ray diffraction—and developed at the Laboratoire National des Champs Magnétiques Intenses (Toulouse, France)—was used. This magnet delivers long-duration (rise time of 16.5 ms, total duration of 60 ms) pulsed magnetic fields—perpendicular to

*Corresponding author: fabienne.duc@lncmi.cnrs.fr

TABLE I. Scattering angles of selected Bragg reflections of $Fe_{1.1}Te$ at temperatures $T < T_N$ (monoclinic $P2_1/m$ phase) and $T > T_N$ (tetragonal $P4/nmm$ phase). The angles were calculated for $E = 31$ keV using the lattice parameters from Ref. [25].

(hkl)	2θ (deg) $T < T_N$ (monoclinic $P2_1/m$)	2θ (deg) $T > T_N$ (tetragonal $P4/nmm$)
(404)	28.21	28.47
$(40\bar{4})$	28.50	28.47
$(044)/(04\bar{4})$	28.62	28.47

the horizontal diffraction plane—up to 31 T, at temperatures from 1.6 to 300 K. A photon energy of $E = 31$ keV ($\lambda = 0.40$ Å) allowed observing Bragg reflections with relatively high Miller indices, as discussed below. Further details about the experimental configuration can be found in Ref. [31].

III. RESULTS AND DISCUSSION

The structural transition from the high temperature, $T > T_N$ tetragonal phase (space group $P4/nmm$) to the low temperature monoclinic phase ($P2_1/m$) leads to a splitting of the (404) Bragg reflection, see Table I. Below T_N we clearly resolve the different scattering angles of the monoclinic (404), $(40\bar{4})$, and the degenerate $(044)/(04\bar{4})$ reflections, as displayed in Fig. 1 by the temperature dependence of the diffracted intensity measured in the absence of magnetic field.

Above T_N these four reflections are degenerated and consequently only one single line is observed. We note that the scattering angle of the tetragonal (404) reflection almost coincides with that of the monoclinic $(40\bar{4})$ reflection. At $T < T_N$, the three reflections (404), $(40\bar{4})$, and (044) are observed in the same frame because of the formation of monoclinic domains with different orientations [16,18,32]: (404) and $(40\bar{4})$ are the signatures of domains whose scattering plane is (**a**,**c**), while (044) is the signature of domains whose scattering plane is (**b**,**c**). Here we detected the phase transition at $T_N \simeq 58$ K and we extracted the refined lattice parameters $a = b = 3.809(2)$ Å and $c = 6.235(5)$ Å in the tetragonal phase, and $a = 3.833(1)$ Å, $b = 3.783(1)$ Å, and $c = 6.262(5)$ Å ($\beta = 89.28°$) in the monoclinic phase, in agreement with previous studies [25,26].

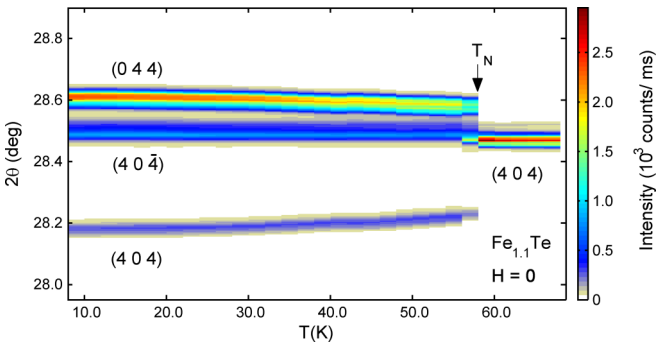

FIG. 1. Temperature dependence of the diffracted intensity of (404), $(40\bar{4})$, and (044) Bragg reflections. The splitting due to the monoclinic distortion is clearly observed at $T_N = 58$ K.

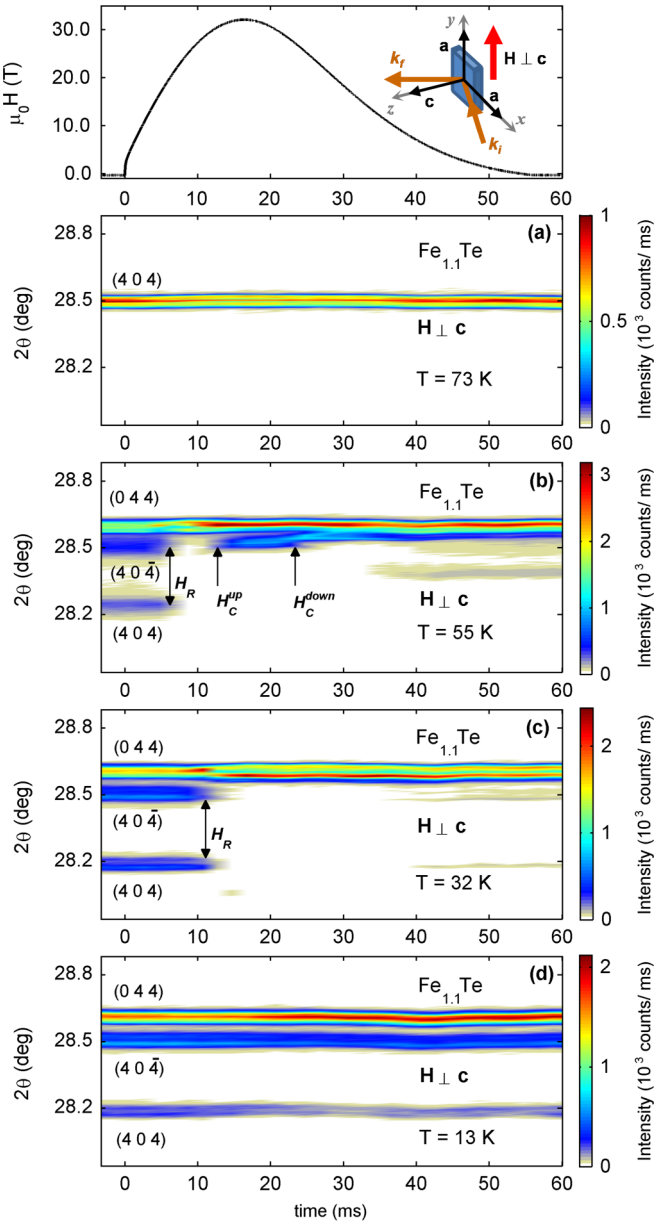

FIG. 2. Time dependence of the diffracted intensity of the (404), $(40\bar{4})$, and (044) Bragg reflections at the temperatures $T =$ (a) 73 K, (b) 55 K, (c) 32 K, and (d) 13 K during a 31 T magnetic field pulse. Results presented here are integrated over the full range of γ angle (out-of-diffraction plane component) $\Delta\gamma = \pm 0.5°$ and were obtained in a single magnetic field pulse. Top: Trace of a 31 T magnetic-field pulse and drawing of the scattering geometry showing the direction of the applied magnetic field and the crystal axes in the high temperature tetragonal phase.

The effect of magnetic fields up to 31 T on the (404), $(40\bar{4})$, and (044) Bragg reflections is shown in Figs. 2 and 3. Due to the constraints of the pulsed field device [31], the diffraction condition at high temperature was kept for the measurements at low temperature and high fields. As the experiment was set up with the scattering vector parallel to the tetragonal [4 0 4] direction, the different monoclinic domains were slightly tilted with respect to the ideal diffraction condition, leading to reflec-

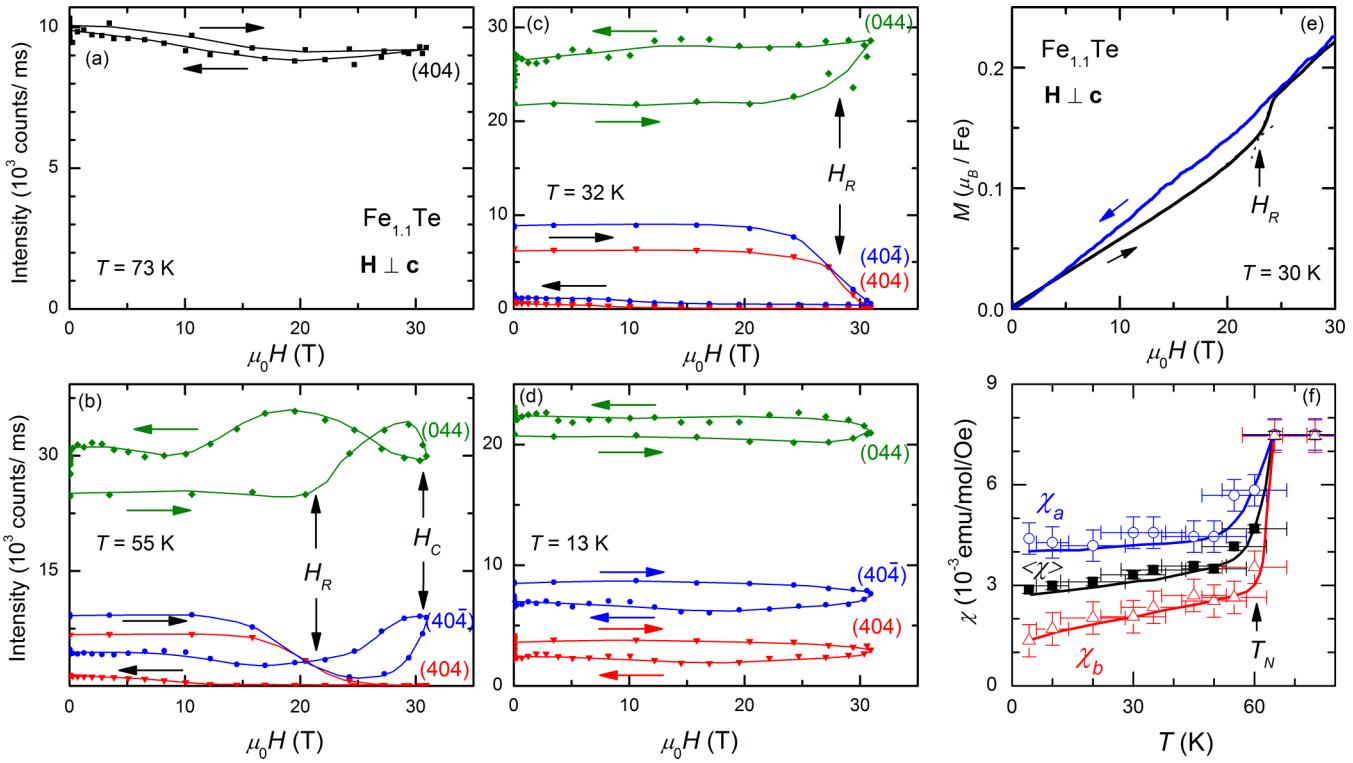

FIG. 3. Field dependence of the diffracted intensity of the (404), (40$\bar{4}$), and (044) Bragg reflections at the temperatures T = (a) 73 K, (b) 55 K, (c) 32 K, and (d) 13 K. (e) Field dependence of the magnetization up to 30 T at $T = 30$ K. (f) Temperature dependence of the magnetic susceptibility, where $\langle\chi\rangle$ and χ_a are estimated from the rise and fall, respectively, of pulsed-field measurements, and where χ_b is estimated assuming a half-half repartition of the domains.

tions with weaker intensities than expected but with relative intensity ratios preserved from one temperature to another.

In Figs. 2 and 3 data are shown for four temperatures to illustrate the behavior in different regions of the phase diagram:

(i) At $T = 73$ K $\gtrsim T_N$, one Bragg peak corresponding to the degenerated tetragonal (404) reflection is observed [see Figs. 2(a) and 3(a)]. The absence of significant variation in the recorded intensity indicates that the structure is unchanged in a high magnetic field, the sample position being stable with regard to the beam during the field pulse.

(ii) At $T = 55$ K $\lesssim T_N$, the (404) and (40$\bar{4}$) reflections vanish while the (044) reflection is reinforced at $\mu_0 H_R \simeq 20$ T during the field rise [see Figs. 2(b) and 3(b)]. This indicates a crystal detwinning at H_R, with a stabilization of the domains for which the scattering plane is (**b**,**c**), i.e., with **H** ∥ **a**. A second transition is observed at $\mu_0 H_C \approx 30/25$ T (rising/falling field), where modifications in the Bragg intensities occur: the intensity at the (044) reflection decreases, that at the (404) reflection remains equal to zero, while the (40$\bar{4}$) reflection is reinforced. These variations are compatible with the onset of a field-induced restoration of the tetragonal symmetry, for which the degenerated tetragonal reflection reappears. Here, due to an integration window $\Delta(2\theta) = \pm 0.1^\circ$ larger than the separation between the monoclinic (40$\bar{4}$) and tetragonal (404) reflections (see Table I), the increase above H_C of the intensity labeled by (40$\bar{4}$) is caused by the partial restoration of the tetragonal (404) reflection, but not by the monoclinic (40$\bar{4}$) reflection. As seen in Fig. 2(b), the transition at H_C shows a strong hysteresis similar to that observed by magnetization [28]. At the end of the pulse at $T = 55$ K, remaining intensities at the monoclinic (404) and (40$\bar{4}$) reflections indicate that the multidomain state is partly restored. To fully restore the zero-field multidomain monoclinic state, the sample has to be heated above the Néel temperature and then cooled down again.

(iii) At $T = 32$ K, the transition at $\mu_0 H_R \simeq 28$ T [Figs. 2(c) and 3(c)] leads to a well-defined and complete vanishing of the (404) and (40$\bar{4}$) reflections accompanied by a reinforcement of the (044) reflection. This reflects a complete selection of the domains whose scattering plane is (**b**,**c**). After the magnetic field pulse, the crystal remains fully (or almost fully) detwinned, as shown by the intensities of the (404) and (40$\bar{4}$) reflections at the background level.

(iv) At $T = 13$ K, a small field-induced transfer of intensity from the (404) and (40$\bar{4}$) reflections to the (044) reflection is detected, but no transition is identified and the monoclinic symmetry is conserved up to 31 T [Fig. 3(d)]. This result is compatible with the magnetization data, which showed that $\mu_0 H_R$ increases significantly at low temperature, reaching $\simeq$35−40 T at $T = 13$ K [28].

Figure 3(e) presents the magnetization of $Fe_{1.1}Te$ measured with μ_0**H** ⊥ **c** up to 30 T at $T = 30$ K, showing an irreversible steplike variation at $\mu_0 H_R \simeq 23$ T [28]. Here we have found that the transition at H_R is associated with a selection of the domains with **H** ∥ **a**. Knowing that the antiferromagnetic moments $\mathbf{m}_{AF}$ order along **b** at zero magnetic field [23,24], our diffraction experiment confirms that a reorientation of the moments with $\mathbf{m}_{AF} \perp \mathbf{H}$ occurs at H_R, in a similar way to the spin-flop transition of single-domain antiferromagnets.

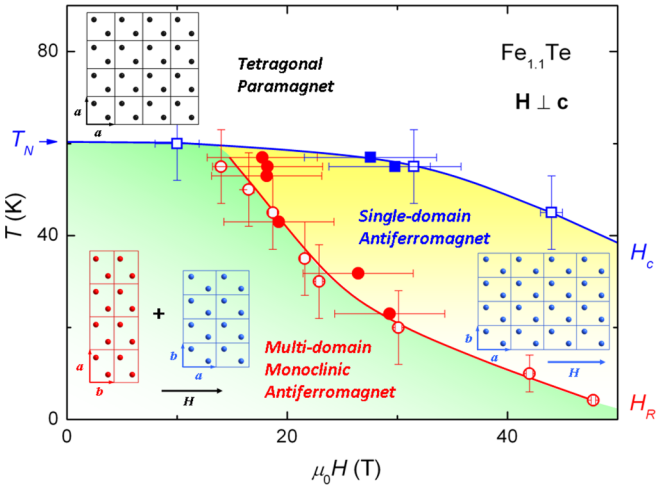

FIG. 4. Magnetic-field-temperature phase diagram of $Fe_{1.1}Te$ with $\mathbf{H} \perp \mathbf{c}$. Closed symbols: Critical fields extracted from x-ray diffraction in field up to 31 T. Open symbols: Critical fields from magnetization measurements from Ref. [28].

Contrary to a spin-flop transition, where the antiferromagnetic moments are aligned perpendicular to the easy axis above the spin-flop field, the moment reorientation observed here corresponds to an alignment of all magnetic moments along their easy-magnetic axis, which is permitted by the domain selection [33]. The specificity of $Fe_{1.1}Te$, in comparison with usual single-domain antiferromagnets, is that the antiferromagnetic state is accompanied by a monoclinic distortion characterized by slightly different values of the lattice parameters a and b (which are equal in the tetragonal paramagnetic state), allowing the magnetoelastic coupling to play a central role in both the domain formation below T_N and the domain selection at the reorientation field H_R. In fields smaller than 30 T, the slope of the linear M versus H curve can be identified as (i), for rising fields, the susceptibility $\langle\chi\rangle$ averaged over the domains, and (ii), for falling fields, the susceptibility χ_a of a single domain with $\mathbf{H} \parallel \mathbf{a}$. Using the rough, but we believe reasonable, approximation of a half-half repartition of domains in the multidomain regime, we approximate by $\chi_b = 2\langle\chi\rangle - \chi_a$ the single-domain magnetic susceptibility for $\mathbf{H} \parallel \mathbf{b}$, and we estimate the intrinsic in-plane anisotropy of the magnetic susceptibility $\chi_a/\chi_b \simeq 3$ of a single domain [see Fig. 3(f)].

These results are synthesized in Fig. 4, where we report the different critical magnetic fields in the whole temperature range. The phase diagram derived from high-field magnetization measurements [28] is also displayed. As in the antiferromagnets $Fe_{1+y}Te_{1-x}S_x$ [16] and $EuFe_2As_2$ [14], our data indicate a partial recovery of the tetragonal symmetry in magnetic fields higher than the antiferromagnetic-to-paramagnetic phase boundary H_C. Interestingly, an irreversible magnetocrystalline domain selection through the magnetoelastic coupling occurs at the moment reorientation field H_R, carrying the b axis in the diffraction plane via a spin-flop-like process. The temperature dependence of H_R is directly related to the mobility of the domain walls. However, an anomalous low-temperature enhancement of H_R is observed (see Fig. 4). It might be explained by a subtle combination of magnetic interactions, in which the magnetic moments on excess off-stoichiometric Fe ions at interstitial sites (which are not equivalent to the main Fe sites) could play a role [34]. Similarly to here, an irreversible (or partly reversible, depending on the temperature) field-induced domain selection was also detected in the Fe-based antiferromagnets $Ba(Fe_{1-x}Co_x)_2As_2$ [12,13] and $EuFe_2As_2$ [15]. In $EuFe_2As_2$, where Eu^{2+} and Fe^{2+} ions are both magnetic, a reorientation of the magnetic moments was observed by magnetization and was identified as the driving force of the persistent detwinning at low field. Magnetization measurements would also be needed in $Ba(Fe_{1-x}Co_x)_2As_2$ to check if a moment reorientation process occurs concomitantly to the detwinning. Interestingly, a reversible domain selection driven by magnetoelastic effects has been detected in the quasi-two-dimensional antiferromagnet $BaNi_2V_2O_8$ under magnetic field [35] as well as in AFe_2As_2 (A = Ba, Ca) compounds under uniaxial pressure [9,11].

Having shown that field-induced detwinning of the antiferromagnet $Fe_{1.1}Te$ is microscopically associated with a reorientation of the antiferromagnet moments, several questions remain and are beyond the scope of this paper. How does the modified distribution of magnetic moment directions affect the breaking of crystal lattice symmetry? Which force drives the magnetic-field-induced detwinning of nematic paramagnets? In the future, studies of the magnetoelastic coupling should be extended to a large class of Fe-based and cuprate materials close to their superconducting instability to better understand the respective roles of magnetism and lattice properties for the development of high-temperature superconductivity.

ACKNOWLEDGMENTS

The authors thank C. Meingast, S. Kasahara, S. Capponi, and M. Mambrini for very useful discussions. The ESRF is greatly acknowledged for granting the beam time for these experiments. The safety issues were addressed with the help of ESRF Safety Group. The MAXIPIX photon-counting pixel detector was lent to the authors by the ESRF detector pool. Part of this work was funded by the ANR Grants No. ANR-05-BLAN-0238 and No. ANR-10-0431 and by the program Investissements d'Avenir ANR-11-IDEX-0002-02 (reference ANR-10-LABX-0037-NEXT).

[1] A. J. Achkar, M. Zwiebler, C. McMahon, F. He, R. Sutarto, I. Djianto, Z. Hao, M. J. P. Gingras, M. Hücker, G. D. Gu, A. Revcolevschi, H. Zhang, Y.-J. Kim, J. Geck, and D. G. Hawthorn, Science **351**, 576 (2016).

[2] R. M. Fernandes, A. V. Chubukov, and J. Schmalian, Nat. Phys. **10**, 97 (2014).

[3] T. Shimojima, Y. Suzuki, T. Sonobe, A. Nakamura, M. Sakano, J. Omachi, K. Yoshioka, M. Kuwata-Gonokami, K. Ono, H. Kumigashira, A. E. Böhmer, F. Hardy, T. Wolf, C. Meingast, H. v. Löhneysen, H. Ikeda, and K. Ishizaka, Phys. Rev. B **90**, 121111 (2014).

[4] T. M. McQueen, A. J. Williams, P. W. Stephens, J. Tao, Y. Zhu, V. Ksenofontov, F. Casper, C. Felser, and R. J. Cava, Phys. Rev. Lett. **103**, 057002 (2009).

[5] A. E. Böhmer, T. Arai, F. Hardy, T. Hattori, T. Iye, T. Wolf, H. v. Löhneysen, K. Ishida, and C. Meingast, Phys. Rev. Lett. **114**, 027001 (2015).

[6] H. Schmid, E. Burkhardt, B. N. Sun, and J.-P. Rivera, Physica C **157**, 555 (1989).

[7] F. Gugenberger, C. Meingast, G. Roth, K. Grube, V. Breit, T. Weber, H. Wühl, S. Uchida, and Y. Nakamura, Phys. Rev. B **49**, 13137 (1994).

[8] A. N. Lavrov, S. Komiya, and Y. Ando, Nature (London) **418**, 385 (2002).

[9] M. A. Tanatar, E. C. Blomberg, A. Kreyssig, M. G. Kim, N. Ni, A. Thaler, S. L. Bud'ko, P. C. Canfield, A. I. Goldman, I. I. Mazin, and R. Prozorov, Phys. Rev. B **81**, 184508 (2010).

[10] J.-H. Chu, J. G. Analytis, K. De Greve, P. L. McMahon, Z. Islam, Y. Yamamoto, and I. R. Fisher, Science **329**, 824 (2010).

[11] I. R. Fisher, L. Degiorgi, and Z. X. Shen, Rep. Prog. Phys. **74**, 124506 (2011).

[12] J.-H. Chu, J. G. Analytis, D. Press, K. De Greve, T. D. Ladd, Y. Yamamoto, and I. R. Fisher, Phys. Rev. B **81**, 214502 (2010).

[13] J. P. C. Ruff, J.-H. Chu, H.-H. Kuo, R. K. Das, H. Nojiri, I. R. Fisher, and Z. Islam, Phys. Rev. Lett. **109**, 027004 (2012).

[14] Y. Xiao, Y. Su, W. Schmidt, K. Schmalzl, C. M. N. Kumar, S. Price, T. Chatterji, R. Mittal, L. J. Chang, S. Nandi, N. Kumar, S. K. Dhar, A. Thamizhavel, and T. Brueckel, Phys. Rev. B **81**, 220406 (2010).

[15] S. Zapf, C. Stingl, K. W. Post, J. Maiwald, N. Bach, I. Pietsch, D. Neubauer, A. Löhle, C. Clauss, S. Jiang, H. S. Jeevan, D. N. Basov, P. Gegenwart, and M. Dressel, Phys. Rev. Lett. **113**, 227001 (2014).

[16] M. Tokunaga, T. Kihara, Y. Mizuguchi, and Y. Takano, J. Phys. Soc. Jpn. **81**, 063703 (2012).

[17] J. Jiang, C. He, Y. Zhang, M. Xu, Q. Q. Ge, Z. R. Ye, F. Chen, B. P. Xie, and D. L. Feng, Phys. Rev. B **88**, 115130 (2013).

[18] T. Nakajima, T. Machida, H. Kariya, D. Morohoshi, Y. Yamasaki, H. Nakao, K. Hirata, T. Mochiku, H. Takeya, S. Mitsuda, and H. Sakata, Phys. Rev. B **91**, 205125 (2015).

[19] A. Cano, M. Civelli, I. Eremin, and I. Paul, Phys. Rev. B **82**, 020408 (2010).

[20] I. Paul, A. Cano, and K. Sengupta, Phys. Rev. B **83**, 115109 (2011).

[21] F.-C. Hsu, J.-Y. Luo, K.-W. Yeh, T.-K. Chen, T.-W. Huang, P. M. Wu, Y.-C. Lee, Y.-L. Huang, Y.-Y. Chu, D.-C. Yan, and M.-K. Wu, Proc. Natl. Acad. Sci. USA **105**, 14262 (2008).

[22] M. H. Fang, H. M. Pham, B. Qian, T. J. Liu, E. K. Vehstedt, Y. Liu, L. Spinu, and Z. Q. Mao, Phys. Rev. B **78**, 224503 (2008).

[23] W. Bao, Y. Qiu, Q. Huang, M. A. Green, P. Zajdel, M. R. Fitzsimmons, M. Zhernenkov, S. Chang, M. Fang, B. Qian, E. K. Vehstedt, J. Yang, H. M. Pham, L. Spinu, and Z. Q. Mao, Phys. Rev. Lett. **102**, 247001 (2009).

[24] S. Li, C. de la Cruz, Q. Huang, Y. Chen, J. W. Lynn, J. Hu, Y.-L. Huang, F.-C. Hsu, K.-W. Yeh, M.-K. Wu, and P. Dai, Phys. Rev. B **79**, 054503 (2009).

[25] E. E. Rodriguez, C. Stock, P. Zajdel, K. L. Krycka, C. F. Majkrzak, P. Zavalij, and M. A. Green, Phys. Rev. B **84**, 064403 (2011).

[26] S. Rößler, D. Cherian, W. Lorenz, M. Doerr, C. Koz, C. Curfs, Y. Prots, U. K. Rößler, U. Schwarz, S. Elizabeth, and S. Wirth, Phys. Rev. B **84**, 174506 (2011).

[27] I. A. Zaliznyak, Z. J. Xu, J. S. Wen, J. M. Tranquada, G. D. Gu, V. Solovyov, V. N. Glazkov, A. I. Zheludev, V. O. Garlea, and M. B. Stone, Phys. Rev. B **85**, 085105 (2012).

[28] W. Knafo, R. Viennois, G. Ballon, X. Fabrèges, F. Duc, C. Detlefs, J. Léotin, and E. Giannini, Phys. Rev. B **87**, 020404 (2013).

[29] R. Viennois, E. Giannini, D. van der Marel, and R. Černý, J. Solid State Chem. **183**, 769 (2010).

[30] C. Ponchut, J. Rigal, J. Clément, E. Papillon, A. Homs, and S. Petitdemange, J. Instrum. **6**, C01069 (2011).

[31] F. Duc, X. Fabrèges, T. Roth, C. Detlefs, P. Frings, M. Nardone, J. Billette, M. Lesourd, L. Zhang, A. Zitouni, P. Delescluse, J. Béard, J. P. Nicolin, and G. L. J. A. Rikken, Rev. Sci. Instrum. **85**, 053905 (2014).

[32] M. Enayat, Z. Sun, U. R. Singh, R. Aluru, S. Schmaus, A. Yaresko, Y. Liu, C. Lin, V. Tsurkan, A. Loidl, J. Deisenhofer, and P. Wahl, Science **345**, 653 (2014).

[33] In single-domain and slightly anisotropic antiferromagnets, a magnetic field applied along the easy magnetic axis usually leads to a spin-flop alignment of the antiferromagnetic moments along a hard magnetic axis perpendicular to the field. In multidomain and slightly anisotropic antiferromagnets, the application of a magnetic field in the easy plane also leads to an alignment of the antiferromagnetic moments perpendicular to the field, but is accompanied by a domain selection permitting all antiferromagnetic moments to remain along the easy magnetic axis. A spin-flop-like moment reorientation is, thus, driving the field-induced domain selection in this class of multidomain and slightly anisotropic antiferromagnets.

[34] X. Fabrèges, I. Mirebeau, P. Bonville, S. Petit, G. Lebras-Jasmin, A. Forget, G. André, and S. Pailhès, Phys. Rev. B **78**, 214422 (2008).

[35] W. Knafo, C. Meingast, K. Grube, S. Drobnik, P. Popovich, P. Schweiss, P. Adelmann, T. Wolf, and H. v. Löhneysen, Phys. Rev. Lett. **99**, 137206 (2007).